

Journal of Geophysical Research: Atmospheres

RESEARCH ARTICLE

10.1029/2017JD027930

Key Points:

- Lightning and precipitation verification procedures
- Explicit lightning forecasting outperforms empirically derived diagnostics

Correspondence to:S. Dafis,
sdafis@noa.gr**Citation:**

Dafis, S., Fierro, A., Giannaros, T. M., Kotroni, V., Lagouvardos, K., & Mansell, E. (2018). Performance evaluation of an explicit lightning forecasting system. *Journal of Geophysical Research: Atmospheres*, 123, 5130–5148. <https://doi.org/10.1029/2017JD027930>

Received 20 OCT 2017

Accepted 1 MAY 2018

Accepted article online 14 MAY 2018

Published online 24 MAY 2018

Performance Evaluation of an Explicit Lightning Forecasting System

S. Dafis¹ , A. Fierro² , T. M. Giannaros¹, V. Kotroni¹, K. Lagouvardos¹, and E. Mansell³ ¹National Observatory of Athens, Institute for Environmental Research and Sustainable Development, Athens, Greece,²Cooperative Institute for Mesoscale Meteorological Studies, University of Oklahoma, Norman, OK, USA, ³NOAA/OAR/National Severe Storms Laboratory, Norman, OK, USA

Abstract In this study, an explicit electrification and lightning parameterization scheme implemented within the Weather Research and Forecasting model (E-WRF, Fierro et al., 2013, <https://doi.org/10.1175/MWR-D-12-00278.1>) is evaluated against selected lightning diagnostic schemes. Convection-permitting simulations of 10 high-impact weather case studies over Greece are compared against lightning observations from the ZEUS ground-based lightning detection network. The model's ability to accurately simulate these convective events is first evaluated through statistical scores of accumulated rainfall. The simulated flash origin density (FOD) fields are then assessed using statistical neighborhood methods. Overall, the simulated FOD fields have good agreement with the observations. Most of the lightning activity over the sea, however, is generally poorly forecasted. Lightning-producing events over the sea near Greece mainly occur during the cold season. Thus, lightning forecast with E-WRF appear to have better skill during the warm season. The simulated areal coverage of FOD using E-WRF also reduces the false alarms of lightning activity both over land and sea compared to a well-documented diagnostic lightning prediction scheme. Given its relatively low computational cost, these results support the potential use of E-WRF for real-time lightning predictions at convection-allowing scales.

1. Introduction

Accurate numerical forecasting of lightning remains a challenging endeavor owing to limited knowledge of the details of storm electrification and errors in predicting the underlying variables (i.e., MacGorman & Rust, 1998). The expansion and improvements of ground-based lightning detection systems has benefitted many areas around the globe with continuous observations of lightning activity (mainly consisting of cloud-to-ground (CG) flashes, i.e., Rudlosky & Shea, 2013; Rudlosky et al., 2017). Following the recent successful launch of the Geostationary Operational Environmental Satellite "R" series (Goodman et al., 2012) with its Geostationary Lightning Mapper (GLM), and the upcoming launch of the Meteosat Third Generation-I satellite with the Lightning Imager, scientists will have an unprecedented access to total lightning data (CG + intracloud [IC] flashes) globally, with high spatiotemporal resolution (i.e., 8–12 km for GLM, Goodman et al., 2013). Similar technologies were also recently made available with the FengYun-4 Geostationary Satellite over China, the western Pacific, and the Indian Ocean (Yang et al., 2017). Such data sets are particularly valuable for evaluating convective-scale forecasts using numerical weather prediction models in regions suffering from poor radar data coverage (i.e., oceans or mountainous areas).

CG lightning remains a hazard worldwide owing to its association with wildfires, fatalities, and damage to electrical infrastructure, whereas IC and CG lightning both pose a threat to aviation (Morgan et al., 2012). Given that cloud electrification arises from complex interactions of microphysical and dynamical processes (Fierro et al., 2006; MacGorman & Rust, 1998; Mansell et al., 2005; Saunders & Peck, 1998; Takahashi, 1978), mixed-phase deep moist convection exhibits notable variability in their lightning evolution, patterns, and intensity. Recent studies have shown that certain lightning behavior/patterns can provide valuable information about the potential severity of thunderstorms (MacGorman & Rust, 1998; Wiens et al., 2005). For instance, Williams et al. (1999) and Schultz et al. (2011) showed that "lightning jumps" (i.e. sudden increases of total or IC flash rates) are well correlated with an increased potential for severe weather events. A decrease in total lightning flash rate, however, cannot reliably indicate the weakening of a storm (Metzger & Nuss, 2013). Ribaud et al. (2015) investigated a bow echo mesoscale convective system during the Hydrological Cycle in the Mediterranean Experiment field campaign in 2012 (Drobinski et al., 2014), using polarimetric radar observations and a portable Lightning Mapping Array (Rison et al., 1999) to provide an insight of the

microphysical species and kinematics that lead to lightning initiation and propagation. They supported the long-known association between lightning, graupel regions, and ice areas within thunderstorms. Karagiannidis et al. (2016) employed Meteosat brightness temperature and the ZEUS lightning detection system (Kotroni & Lagouvardos, 2008) to analyze 92 thunderstorms over Greece and showed that a cloud top temperature of at least -20°C and an average rapid ambient temperature drop of $11^{\circ}\text{C}/5\text{ min}$ is required to observe CG lightning.

The three-dimensional compressible nonhydrostatic Weather Research and Forecasting Model (WRF; version 3.7) with Advanced Research WRF dynamic solver (WRF-ARW; Skamarock & Klemp, 2008) has been broadly used for studying and forecasting all types of weather events. Despite its extensive usage, only a few studies focused on explicit lightning forecasting, primarily because the operational usage of most explicit schemes, which include more complex discharge physics (i.e., Mansell et al., 2005; Pinty & Barthe, 2008), remain computationally more expensive and comparatively more challenging to implement than diagnostic schemes. Lightning diagnostic schemes, which produce bulk flash metrics such as flash rates per area or flash origin density rates, employ empirically derived statistical methods or relationships with diagnosed microphysical and kinematic properties of thunderstorms. Often, some of these functional relationships are based on observations. One of the most widely used diagnostic schemes was developed by McCaul et al. (2009), which utilizes the updraft mass flux of graupel within a specific layer combined with vertically integrated ice mass to diagnose total flash rates in the convective and stratiform regions of storms. Yair et al. (2010) proposed a lightning potential index scheme based on potential charge separation, while Lynn et al. (2012) introduced the potential electrical energy to predict CG and IC lightning in convection-allowing simulations ($\Delta x = 3\text{--}4\text{ km}$). Wong et al. (2013) revised the Price and Rind (1992) diagnostic lightning parameterization, but this algorithm (PR92) requires a cumulus parameterization and, thus, cannot be applied to cloud-scale simulations.

Giannaros et al. (2015) evaluated the performance of PR92 over Greece by conducting WRF simulations of 10 case studies. They suggested several adaptations to PR92 to lessen a systematic positive bias in lightning occurrence, mostly attributed to an overestimation of the mass mixing ratios of mixed-phase hydrometeors by the microphysics schemes used in their study (Purdue-Lin/WSM6/Thompson). Giannaros et al. (2016) presented the results of 1 year operational forecasting of lightning activity in Europe, by implementing a modified version of PR92, showing a strong dependence of the algorithm's performance to the convective parameterization scheme used. Pytharoulis et al. (2016) investigated the performance of the lightning potential index algorithm for an extreme precipitation event in north Greece by comparing lightning occurrence against the ZEUS network CG observations over a 24-hr period. Their sensitivity experiments of topographical variations in elevation during a period of strong synoptic forcing also revealed a noteworthy influence of the convective parameterization scheme used on the spatial and temporal evolution of lightning activity.

Fierro et al. (2013) implemented a computationally inexpensive, explicit lightning forecasting scheme within WRF-ARW (hereafter E-WRF), whose performance was evaluated over a wide variety of convective regimes. In this study, we make use of E-WRF to evaluate its performance for 10 single-day events over Greece between 2010 and 2013 and to investigate the skill of explicit lightning forecasting at convection-allowing scales. The same 10 single-day events have been analyzed in Giannaros et al. (2015), and, thus, the current study also offers the opportunity to compare the skill between explicit lightning forecasting and lightning forecasting based on the empirically calibrated diagnostic algorithm from PR92. Additionally, the McCaul et al. (2009) lightning prediction scheme (MC), which has been used as the operational lightning forecasting product of the National Severe Storms Laboratory (NSSL) WRF forecasts, is also evaluated and compared against the explicit forecasting scheme (E-WRF). Lightning forecasts are dependent on the model's ability to accurately simulate the placement and timing of the observed storms. To evaluate this more basic criterion, numerical simulations are compared against precipitation observations from 140 rain gauges and ZEUS lightning observations (no radar data are available over Greece). After demonstrating that the observed convection is reasonably reproduced by WRF, the present study will investigate the forecast ability of an explicit lightning model within a numerical weather prediction forecast model such as E-WRF at convection-allowing scales.

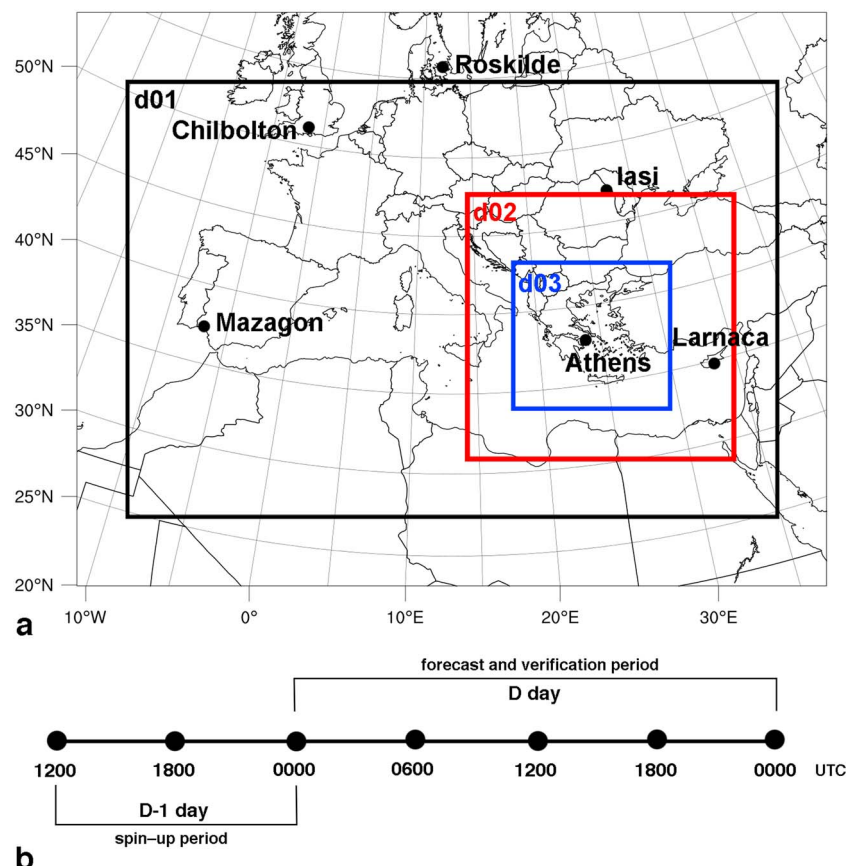


Figure 1. Sketch of the WRF-ARW domains used in this study (a). The parent domain (d01) covers most of Europe and North Africa. The intermediate nested domain (d02) includes the Balkans, South Italy, and Asia Minor, while the convection-allowing, inner nest (d03) covers Greece. The six very low frequency sensors of lightning detection network ZEUS are also marked on the map. (b) Schematic diagram highlighting the spin-up and forecast periods for all the experiments in this study.

2. Model and Data Description

2.1. Simulations Setup

The geographical areas covered by the three simulation domains herein are illustrated in Figure 1a. The parent domain (d01) has a horizontal grid spacing of 24 km (185×125 grid points). The inner domains 2 (d02) and 3 (d03) are one-way nested to d01 and d02, respectively. The horizontal grid spacings for d02 and d03 are 6 km (301×301 grid points) and 2 km ($526 \times$ grid points), respectively. The vertical grid consists of 50 unevenly spaced full sigma levels extending up to a fixed model top set at 50 hPa. Due to the relatively coarse horizontal resolution of d01 and d02, the Grell-Devenyi convective parameterization (Grell & Devenyi, 2002) was activated there, while d03 solely employs explicit microphysics. All simulations were initialized at 1200 UTC on the previous day ($D - 1$ day) and integrated for a 36-hr period, with the first 12 hr considered as the spin-up phase (Figure 1b). Model verification thus focuses on the 24-hr period starting at 0000 UTC (D day). Initial and boundary conditions were derived from the 6-hourly National Centre for Environmental Predictions $1^\circ \times 1^\circ$ 1200 UTC analyses.

The physics options selected include the Noah land surface model (Chen & Dudhia, 2001), the Rapid Radiative Transfer Model (Mlawer et al., 1997), and Dudhia (Dudhia, 1989) schemes for the longwave and shortwave radiation processes, respectively, the Yonsei University (Hong et al., 2006) planetary boundary layer scheme and the MM5 similarity scheme for the surface layer physics (Zhang & Anthes, 1982). The microphysics were parameterized using the two-moment NSSL scheme (Mansell et al., 2010), which is the only scheme thus far coupled with E-WRF. The NSSL microphysics predicts the mass mixing ratios and number concentrations of six bulk hydrometeor species including rain, cloud water, cloud ice, snow, graupel, and hail.

2.2. Overview of E-WRF

The numerical model in this study employs explicit electrification and lightning parameterizations within WRF-ARW (E-WRF; Fierro et al., 2013). Electrification was only activated in the innermost, cloud-resolving domain (d03). To compute charge separation, the Saunders and Peck (1998) noninductive charging scheme and the inductive charging scheme of Mansell et al. (2005) based on Ziegler et al. (1991) were selected. Noninductive charging treats charge separated during rebounding graupel/hail and ice collisions, while polarization/inductive charging considers the charge separated during collisions between cloud water and ice-graupel-hail in the presence of an electric field. Charge separation from ice-ice collisions is assumed to be negligible owing to small differential terminal fall speeds and lack of laboratory experiments (Fierro et al., 2013; Mansell et al., 2005). The magnitude of charge separated within a grid cell is calculated following equation (7) of Mansell et al. (2005). Since the total net charge within the domain should equate 0 (conservation of total charge), the charge gained during inductive and noninductive collisional charging by one of the hydrometeor species involved equals the amount of charge lost by the other.

The electric field in E-WRF is solved iteratively using the message-passing interface, black box multigrid iterative solver BoxMG (Dendy & Moulton, 2010; Dendy, 1987) for three-dimensional nonsymmetric convection-diffusion problems. The boundary condition at the surface is set to zero potential and to fair-weather potential at the top of the domain (Dirichlet boundary conditions), while for the lateral boundary conditions, zero normal derivatives are used with a first-guess solution given by the fair-weather electric field formulation of Gish (1944). The discharge model follows the configuration of Fierro et al. (2013), with 120 kV/m as the vertically constant electrical field threshold for lightning initiation (E_{crit}) and a discharge cylinder with a 6-km radius (centered at the discharge location) extending vertically through the entire depth of the simulation domain. The critical electrical field E_{crit} used in this study follows the Dwyer et al. (2003) break-even field magnitude for middle levels of the troposphere. A preliminary tuning of the model by changing this threshold by ± 10 kV/m showed insignificant changes in flash production. The higher the E_{crit} threshold, the larger the charge buildup required for discharge will be (and vice versa). This threshold was tested during the development of E-WRF and showed overall negligible sensitivity for changes to E_{crit} within 20% (from 120 kV/m). For a more comprehensive description of the electrification physics and lightning parameterizations, the reader is invited to consult Fierro et al. (2013).

McCaul et al. (2009, hereafter MC) introduced a lightning threat diagnostic approach, which utilizes upward fluxes of precipitating ice hydrometeors at a specific height of -15°C to capture the temporal variability of lightning threat within convective regions and the vertically integrated amounts of ice hydrometeors over the full storm depth to represent lightning in stratiform regions. A final blended product, calibrated for the WSM6 microphysics scheme, was devised to forecast lightning threat from the output of cloud-resolving model, which has been evaluated against fine-scale total lightning observations from the Lightning Mapping Array (Fierro et al., 2013; MC). In the present study, the MC method was compared with explicit flash rates from E-WRF. The performance of each method was determined by comparing the resulting forecasts with the lightning observations from the ZEUS network, described below. For the relatively small (regional) simulation domains used in this study, the difference in computational time between explicit electrification and the McCaul scheme was about 10–15%, in line with Fierro et al. (2013).

2.3. Lightning Observations

The lightning observations were provided by the long-range lightning detection network ZEUS (Kotroni & Lagouvardos, 2008). This system consists of six very low frequency sensors composed of six receivers during the study period (2010–2013, Figure 1), namely, Athens (Greece), Chibolton (UK), Roskilde (Denmark), Iasi (Romania), Larnaca (Cyprus), and Mazagon (Spain). Each receiver measures the time rate of change of the vertical component of the electric field from radio emissions of lightning strokes (sferics) in the six very low frequency range (7–15 kHz) and detects a probable candidate using a minimum number of receiver detections for each event. A synchronization of the sampled time series between the different receivers is performed, by using GPS time stamps. Finally, lightning location data are sent to the central station of the network (Athens) using the arrival time difference triangulation technique which defines a hyperbola of possible lightning source positions over the Earth's surface associated with the same arrival time difference (i.e., time-of-arrival technique). The mean detection efficiency for CG lightning is approximately 25% with much lower

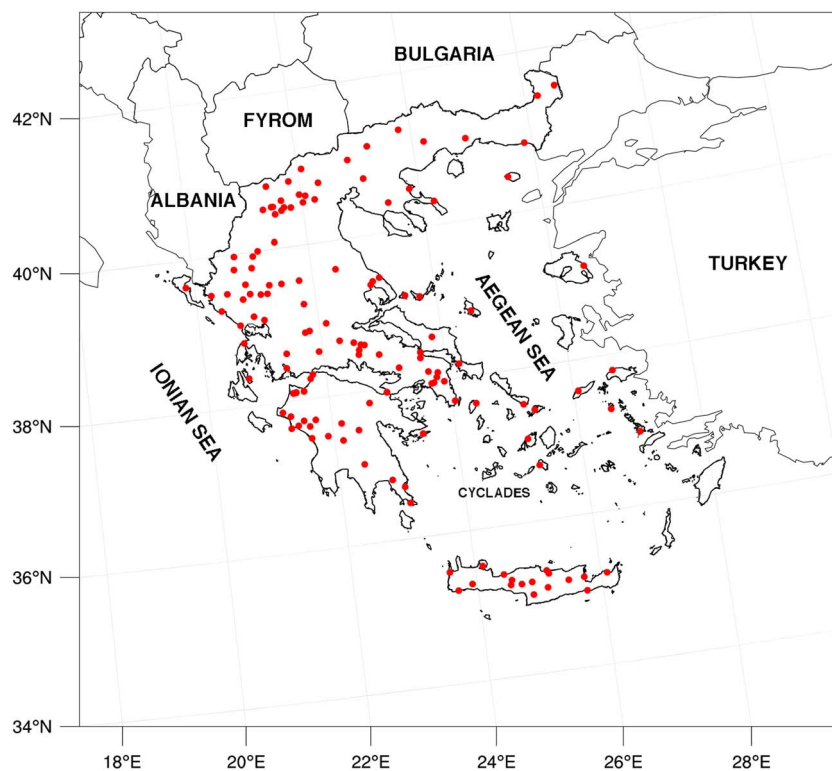


Figure 2. Map highlighting the locations of the 140 rain gauges over Greece (red dots) that are used for forecast verification.

performance (i.e., ~10–20%) during the night than during the day (i.e., 30–50%), and the mean location error is on the order of 6.8 km (Lagouvardos et al., 2009). One important finding in Lagouvardos et al. (2009) was that ZEUS does not miss thunderstorm occurrence, and the majority of strokes have a location difference less than 5 km when compared to the LINET detection network. In terms of detection efficiency and location accuracy, the performance of ZEUS is comparable to other global networks and is therefore deemed sufficiently accurate to provide an initial, broad representation of the occurrence of lightning activity in the Mediterranean. Most importantly, emphasis herein is given to testing the model skill in predicting lightning occurrence rather than the actual number of lightning strokes.

2.4. Precipitation Observations

The first goal of this study is to evaluate the model skill in forecasting the observed convection for the selected 10 cases by analyzing accumulated precipitation fields (as no radar data are yet available over Greece). The 24-hr simulated accumulated precipitation (APCP) for each case study are verified against observations derived from a network of 110–140 rain gauges (Figure 2), which is operated by the National Observatory of Athens (NOA; Lagouvardos et al., 2017). The six model grid points surrounding each rain gauge were considered for the computation of standard qualitative statistical measures including the probability of detection (POD) and the false alarm ratio (FAR; i.e., contingency tables). These forecast metrics first were averaged over all 10 case studies and then classified by the main climate regimes over Greece, namely, the cold period and the warm period. The following APCP thresholds were considered for the contingency table elements: 1, 2.5, 5, 10, and 20 mm. Additionally, the following quantitative measures were calculated: the quantity bias (QB) and the mean absolute error (MAE; Federico et al., 2004; Lagouvardos et al., 2003; Mazarakis et al., 2009). For the quantitative performance metrics, five APCP ranges were used: 0.1–2.5, 2.5–5, 5–10, 10–20, and >20 mm. As a last step, the forecast verification also made use of neighborhood methods (i.e., equitable threat score [ETS]; Clark & Weisman, 2010) to account for potential displacement in the simulated convection using the same APCP thresholds as for FAR/POD with an influence radii ≤ 12 km.

2.5. Selection of the Case Studies

A seasonal categorization has been used to select the case studies. The warm period is defined as the time of year between May and September, when storms over Greece are primarily driven by diurnal heating of the surface rather than synoptic systems (Mazarakis et al., 2008). The cold period in Greece spans the remaining months between October and April, wherein the vast majority of lightning-producing storms arise from synoptic-scale forcing.

2.5.1. Warm-Period Case Studies

Five warm-period case studies were chosen, which produced significant amounts of precipitation (both rain and hail) over a notable portion of Greece (i.e., within d03). The event of 5 June 2010 was characterized by local convection both over land and sea with nine rain gauges reporting more than 30 mm of rainfall in less than 3 hr. The observed lightning activity had two maxima, one around 0300 UTC and the second at 1300 UTC. Three heavy rainfall events were reported in north and central Greece by the European Severe Weather Database (ESWD; Dotzek et al., 2009), which included a waterspout in the NW Aegean Sea. During the second event on 2 July 2010, widespread lightning activity was detected around 1200 UTC with the maximum flash rate recorded by ZEUS just after 1300 UTC. More than 20 mm of rainfall was recorded by 10 rain gauges in northern Greece. On 11 September 2010, a cold front reached the west coasts of Greece and produced strong lightning storms over the Aegean Sea with 24-hr rainfall accumulations exceeding 50 mm for 10 of the gauges in west and central Greece. On 21 September 2011, lightning activity was observed both over land and sea, with 12 rain gauges recording 12-hr rainfall totals in excess of 20 mm. During the last warm-period case on 10 August 2012, several severe weather events were reported by the ESWD, including two waterspouts in central Greece during an early-morning storm associated with intense lightning activity.

2.5.2. Cold-Period Case Studies

On 18 October 2010, two frontal systems affected the innermost (d03) forecast domain. The first produced heavy rainfall in the Cyclades but weak lightning activity, while in contrast, the second cold front later in the day triggered widespread thunderstorm development over the Ionian and Aegean Seas with one reported tornado (rated EF-2). Ten rain gauges recorded more than 50 mm of rainfall in less than 24 hr and over the South Aegean Sea recorded a peak rainfall total of 303 mm (Ikaria). On 12 January 2011, a weak low-pressure system propagated over the Ionian Sea and was associated with pulsating lightning activity, mostly over the sea, with multiple maxima between 0500 and 1500 UTC. APCP amounts in excess of 20 mm were recorded by 14 stations. The heavy precipitation event on 6 February 2012 was associated with a deep low (984 hPa) reaching the west coasts of Greece. Lightning activity was more pronounced near the occlusion of the cyclone in the Ionian Sea, but lightning was also recorded over the mainland of Greece and the Aegean Sea in the late afternoon and at night. Some of the lightning events over mountain ranges were accompanied by heavy snowfall (thundersnow). The quasi-linear mesoscale convective system event of 29 October 2012 was one of the most intense recorded over the last decade according to the ESWD, with 18 reports of hail up to 5 cm in diameter and an EF-2 tornado. Approximately 16,000 lightning strikes were recorded in 24 hr, most of them between 1100 and 1800 UTC over NE Aegean Sea. Finally, on 6 November 2013 a low-pressure system from south Italy moved gradually toward the island of Crete. The cold front produced thunderstorms first in east continental Greece and later over the Aegean Sea. Nine rain gauges recorded APCP >40 mm in a few hours, several severe wind gust events (> 25 m/s) were reported by the ESWD along with one waterspout in the Dodecanese (Astypalaia) that came ashore producing damage to infrastructure.

3. Verification Procedures and Discussion

3.1. Verification of Precipitation

The two nested domains (d02 and d03) were used to evaluate the precipitation forecasts in this study. Because Giannaros et al. (2015) used model settings similar to d02 for the lightning forecast (PR92) of the same 10 high-impact weather cases, this provides an opportunity to compare not only the APCP forecasts but the lightning forecasts as well.

The POD for the 24-hr APCP averaged separately for the warm and cold-period cases are lower for d03 (Figures 3c and 3b) than for d02 (Figures 3a and 3b) across all precipitation thresholds. During both warm

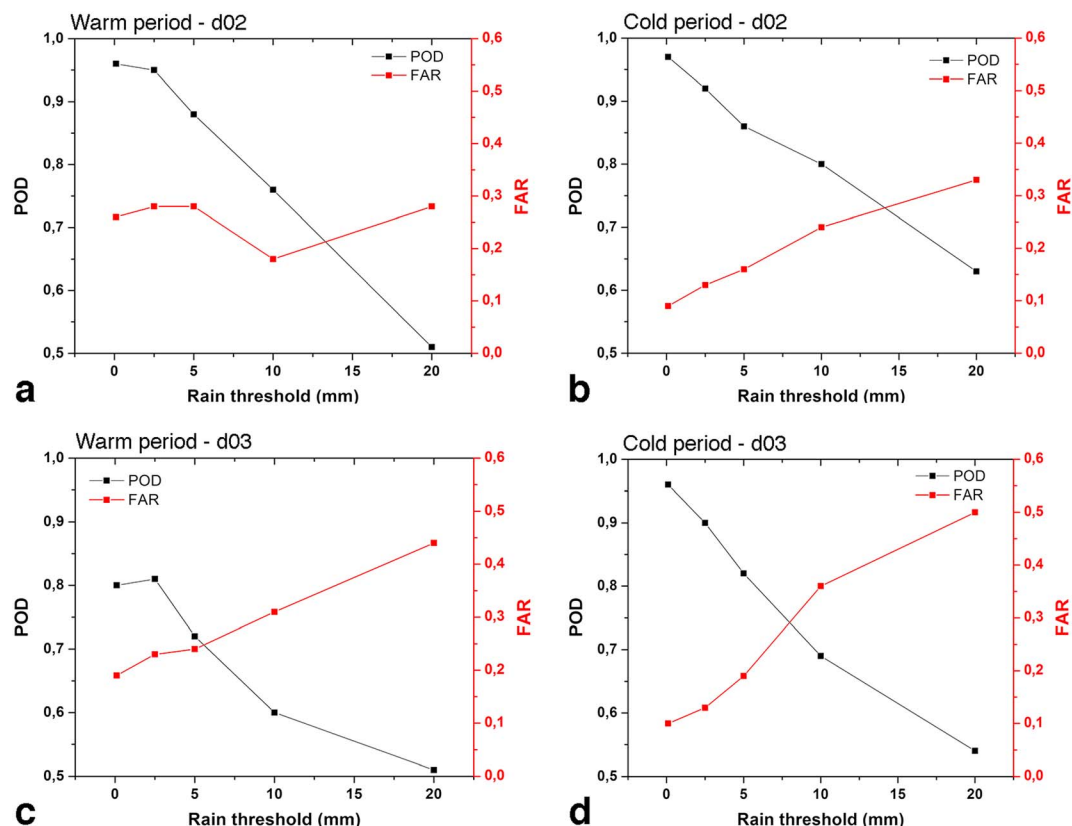


Figure 3. POD and FAR for the 24-hr WRF-simulated precipitation in d02, averaged for (a) the warm-period and (b) the cold-period case studies and in d03 averaged for (c) the warm-period and (d) the cold-period case studies. POD = probability of detection; FAR = false alarm ratio; WRF = Weather Research and Forecasting model; d02 and d03 = inner domains 2 and 3.

and cold periods, the largest (smallest) departure between the two domains is seen for the 10 (20) mm APCP thresholds, respectively. The POD values in Giannaros et al. (2015) are comparable with those for d02 herein, while d03 produces overall lower PODs for APCP thresholds between 1 and 10 mm. Differences in FAR scores for d03 and d02 are similar at low (≤ 5 mm) APCP thresholds. At higher APCP thresholds (i.e., 10 and 20 mm) the FAR is notably larger in d03 (Figures 3c and 3d). Giannaros et al. (2015) study produced lower but comparable FAR values for all precipitation thresholds used, with a maximum difference seen for APCP = 20 mm. Differences in FAR scores between the two studies for APCP ≤ 10 mm remain overall negligible (i.e., ≤ 0.04).

The MAE scores during the warm-period cases (Figures 4a and 4c) are larger across all precipitation ranges with the worst performance seen in predicting the largest precipitation amounts (i.e., ≥ 20 mm). Precipitation forecasts over d02 (Figures 4a and 4b) exhibit MAE scores that are consistent with those of Giannaros et al. (2015) across all APCP thresholds. Weaker performance at predicting precipitation is seen for d03 (Figures 4c and 4d), especially for APCP ≥ 20 mm/24 hr (i.e., Figure 4c). For the QB metric, the most significant difference between d03 and d02 is the underestimation of precipitation in d02 for APCP ≥ 20 mm during the warm period (compare Figures 5a and 5c). When comparing the QB results for d02 (Figures 5a and 5b) against those of Giannaros et al. (2015; their Figure 2), the forecasts in this study produce overall comparable values for all precipitation thresholds (i.e., QB between -2.0 and $+0.6$ mm).

To examine any potential displacement of the precipitation in the forecasts, a more comprehensive statistical evaluation of the precipitation fields in the high-resolution domain (d03) is conducted using neighborhood methods (Casati et al., 2008; Clark & Weisman, 2010; Ebert, 2009; Fierro, Clark, et al., 2015; Roberts & Lean, 2008; Schwartz et al., 2010). First, the ETS for 6-hr APCP intervals is calculated for six neighborhood radii (2, 4, 6, 8, 10, and 12 km) following Clark and Weisman (2010), using the same APCP thresholds as in Figure 4. These ETS scores are then averaged over the entire domain (d03).

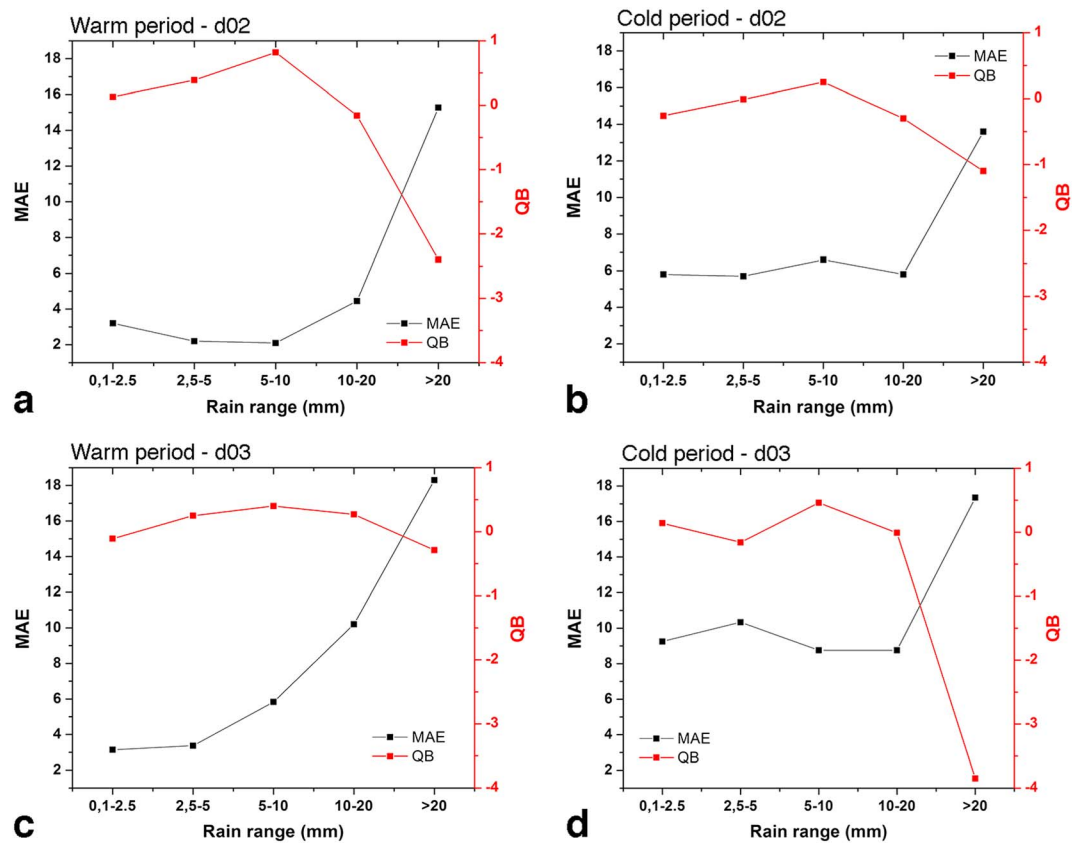


Figure 4. MAE and QB for the 24-hr WRF-simulated precipitation in d02, averaged for (a) the warm-period and (b) the cold-period case studies. (c and d) As in (a) and (b) but for d03. MAE = mean absolute error; QB = quantity bias; WRF = Weather Research and Forecasting model; d02 and d03 = inner domains 2 and 3.

For the warm-period case studies, the ETS for the 6-hourly APCP thresholds of 2.5 mm is significantly improved between 1200 and 1800 UTC (Figure 5a) compared to the first 6 hr of the day. In contrast, for the cold-period cases (Figure 5b), the 1200–1800 UTC period produced the lowest ETS scores (for all radii and APCP thresholds). For the warm cases, increasing the APCP threshold to 5 mm and above results in lower diurnal ETS differences (not shown). The larger the neighborhood radius, the higher the ETS score. This behavior is explained by increasing POD (decreasing FAR) as the radius increases (Fierro, Clark, et al., 2015).

3.2. Verification of Lightning

The verification procedure for lightning was carried out on a dichotomous decision basis, using paired modeled and observed lightning values. Rationale for this procedure is that this work primarily aims at testing the model's skill in predicting lightning occurrence rather than the actual number of lightning strokes. ZEUS lightning observations were aggregated/projected on the 2-km horizontal resolution domain (d03) and then compared with the simulated flash origin density rate (FOD) per grid cell (equation 9 in Fierro et al., 2013). A first verification for the 24-hr FOD values was conducted by constructing contingency tables for two neighborhood radii (2 and 6 km) around each grid point, following Clark and Weisman (2010).

A direct comparison of the simulated FOD with ZEUS-detected spatial and temporal distribution of lightning activity can be made using Figures 6 and 7, which show the grid cells containing at least one flash per hour. The timing and location of the forecast FOD remains generally in good agreement with the ZEUS observations, particularly for the warm-period cases over land (i.e., 2 July 2010 and 10 August 2012). This is not the case for most of the cold-period cases, however, especially over the sea, where E-WRF forecasts lightning over large areas that had little-to-no lightning strikes detected by ZEUS. For the case on 18 October 2010 (Figures 7a and 7b), the forecast FOD over most of continental Greece and the North Aegean Sea is poorly verified by the observations. Also, on 6 November 2013 (Figures 7i and 7j) the model simulates excessive

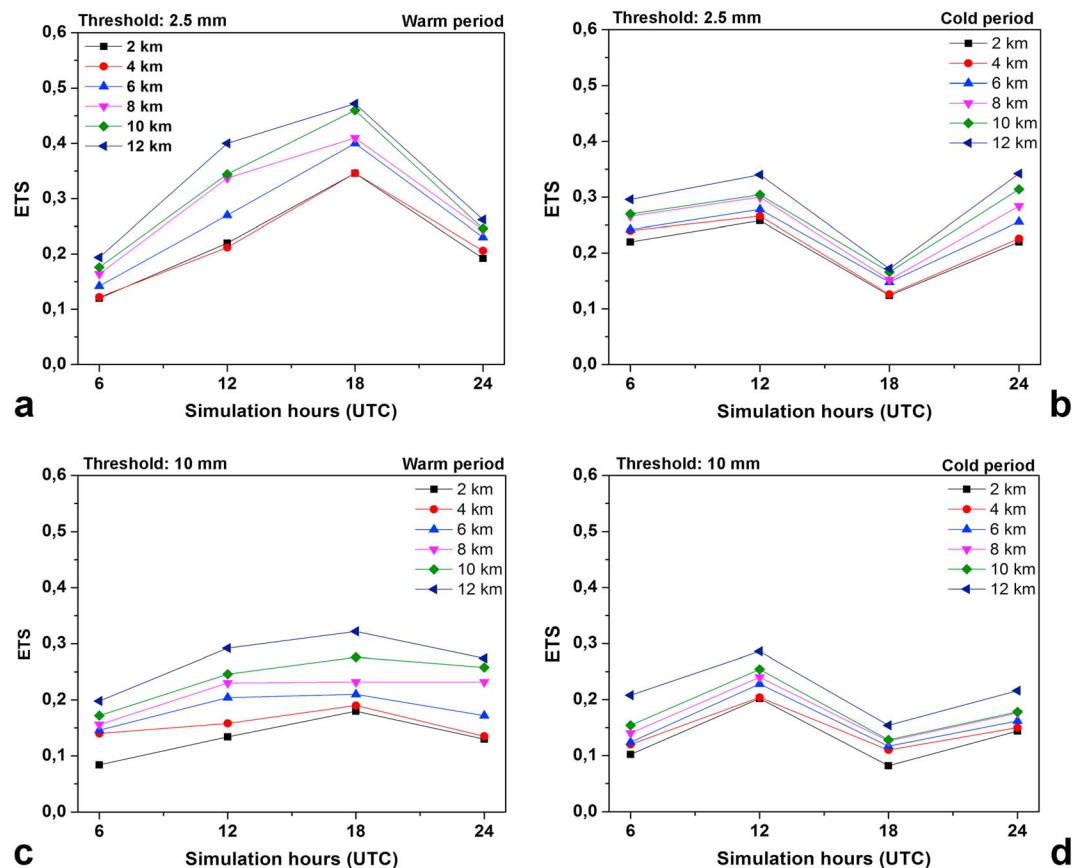


Figure 5. ETS for 6-hourly APCP bins over the 24-hr forecast period for all six neighborhood radii and for two APCP thresholds, averaged for (a, c) the warm-period case studies and (b, d) the cold-period case studies. ETS = equitable threat score; APCP = accumulated precipitation.

lightning activity in the Ionian Sea and continental parts of northern Greece and south Bulgaria where ZEUS detected only a few lightning strikes. The aforementioned case studies also exhibit the lowest ETS values for accumulated precipitation (not shown). The lack of radar observations or any high spatiotemporal observations of convection over the Mediterranean Sea for these cases hinders a more detailed qualitative analysis of the rainfall forecasts.

For most of the case studies, the model produces more grid points containing at least one lightning flash per hour (mostly over the sea) than ZEUS. One potential factor for this apparent overestimation of lightning flash production in the model is the low mean detection efficiency of the ZEUS network (25%). Because the bulk discharge scheme in E-WRF does not discriminate different lightning types (Ziegler & MacGorman, 1994), it is not feasible to determine model error for simulated CG events. Despite this tendency to overestimate flash coverage (Fierro et al., 2013), E-WRF still underpredicted FOD areas for two cases (i.e., 2 July 2010 and 10 August 2012), which corresponds to the smaller-than-observed spatial coverage of thunderstorms (compare Figures 6c, 6d, 6i, and 6j).

This analysis also provides an opportunity to analyze the diurnal cycle of the observed versus simulated lightning activity. For the majority of the warm-period cases, the model simulates FODs a few hours later than observed over continental Greece. For the cold-period cases frontal weather systems are associated with a distinct diurnal cycle in lightning activity, with a bias of only a few hours between model and observations.

In summary, it is challenging to provide accurate estimation of lightning forecast error because of the inherent convolution between model error and the observational systematic error arising from ZEUS (low detection efficiency). Complicating the problem further is the inherent sensitivity of the simulated lightning to collection/collisions efficiencies of graupel-ice and ice concentration thresholds (Fierro, Mansell, et al., 2015; Fierro et al., 2006; Mansell et al., 2005).

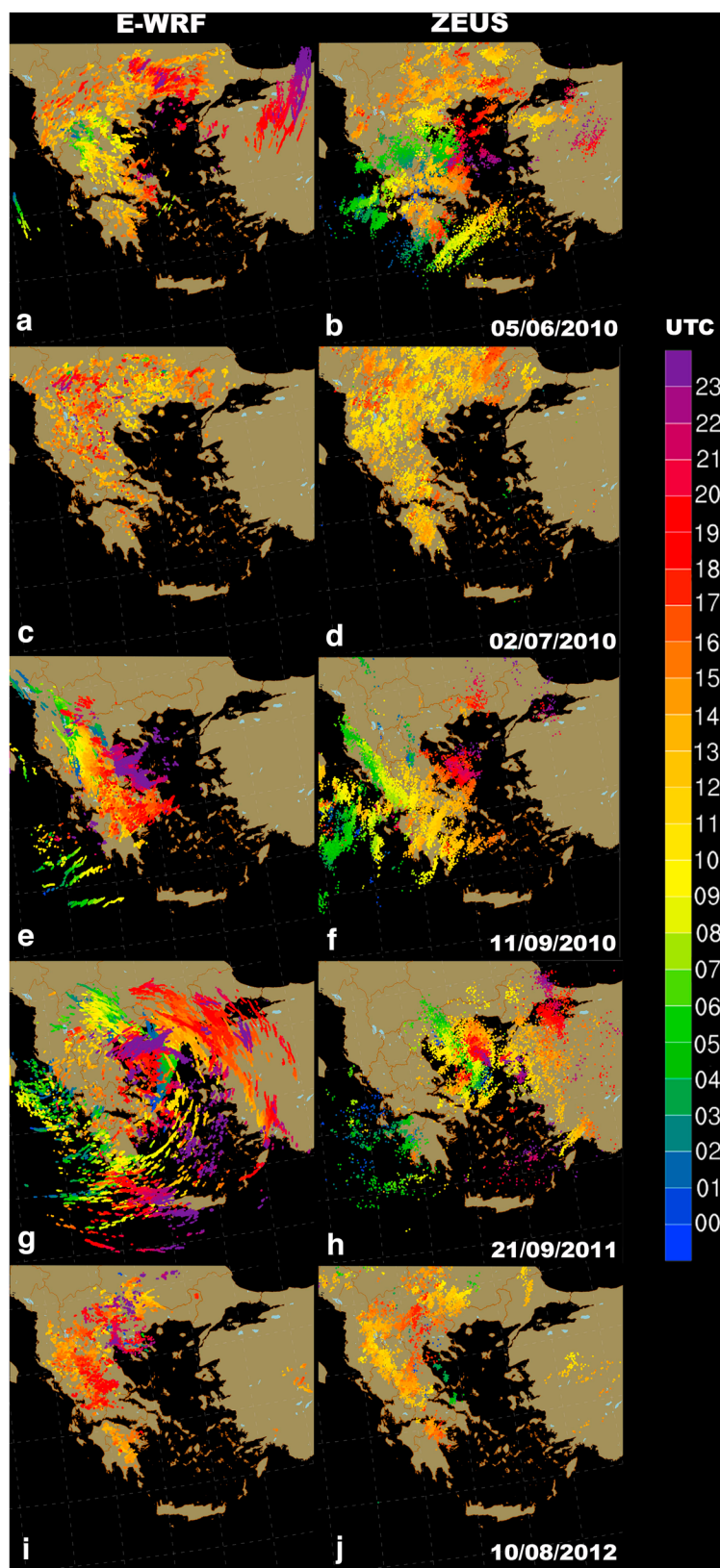


Figure 6. Hourly simulated FOD by E-WRF (left column—a, c, e, g, i) and lightning strikes detected by ZEUS (right column—b, d, f, h, j) for the five warm-period case studies. The colored shadings on the right of the figure indicate the corresponding 1-hr accumulation intervals. FOD = flash origin density; E-WRF = explicit lightning forecasting scheme within the Weather Research and Forecasting model.

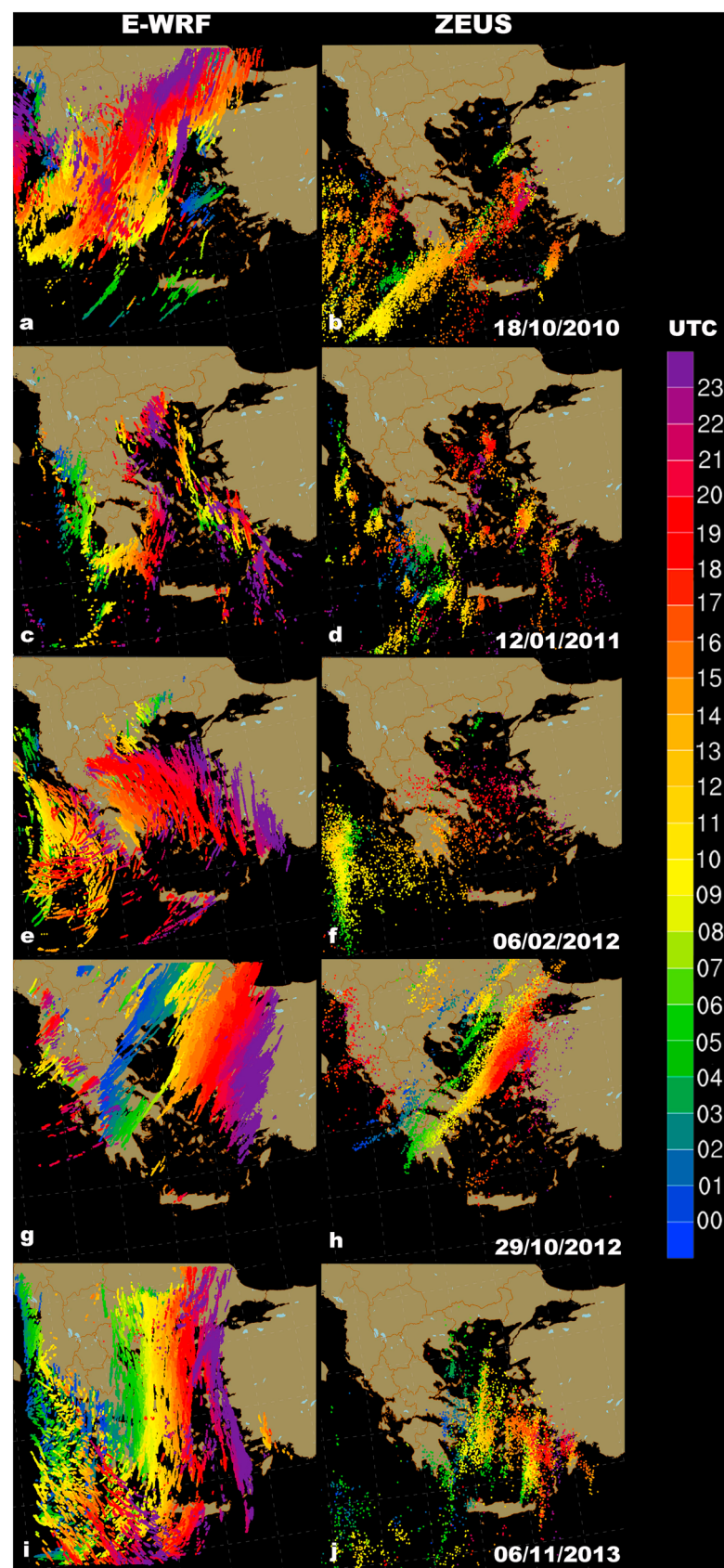


Figure 7. As in Figure 6, but for cold-period cases.

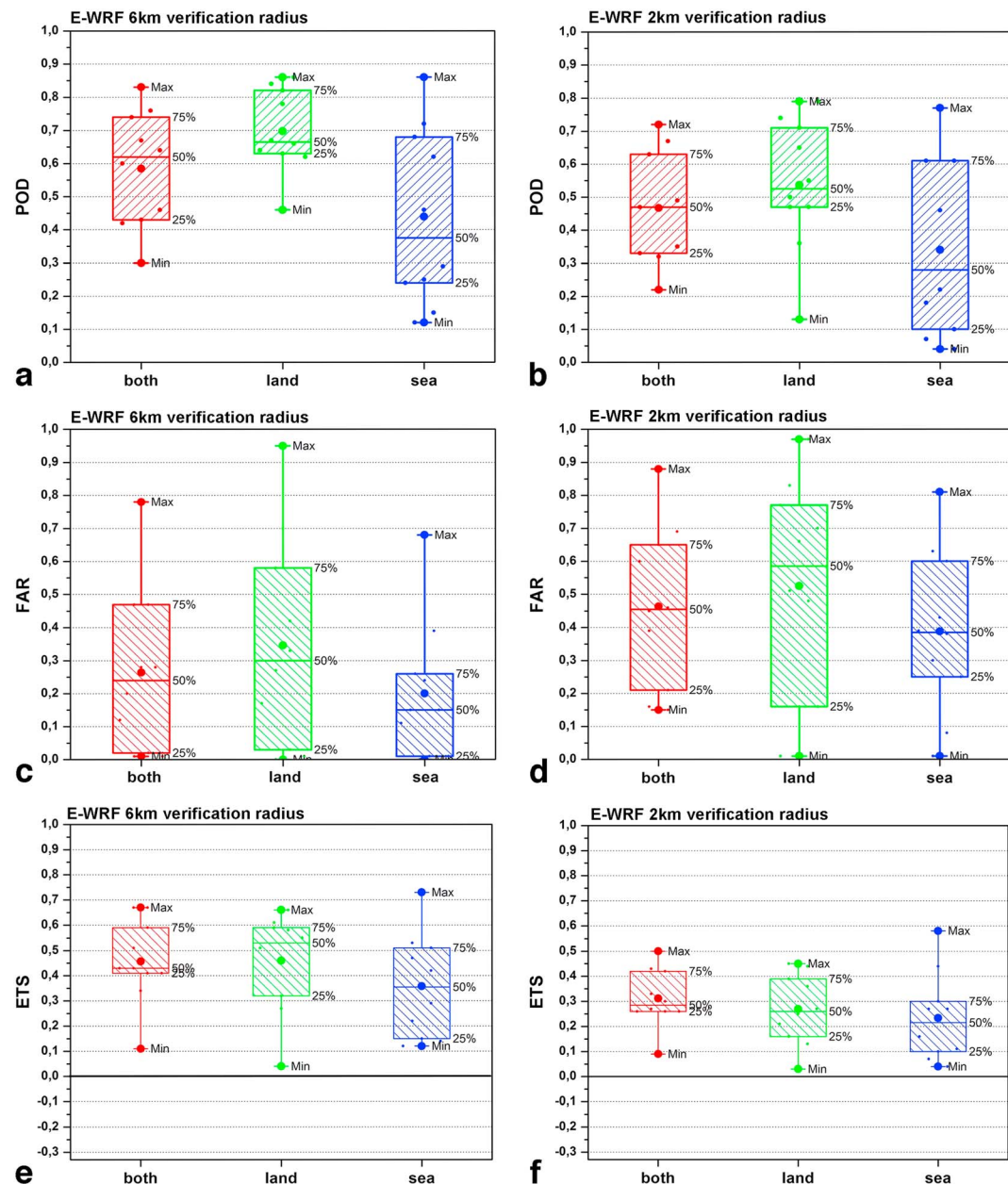


Figure 8. Box and whisker plots of (a, b) POD, (c, d) FAR and (e, f) ETS for the 24-hr accumulated FOD from E-WRF for (a, c, e) 6 km and (b, d, f) 2 km neighborhood radii, for the 10 case studies. Each small colored dot represents the statistical scores of each case study, and the large dot inside the box represents the mean score. The 50% line within the box depicts the median correlation. The boxes are delimited by the lower and upper quartiles (25th and 75th). The 2.5th and 97.5th percentile values are shown at the end bars of the dotted lines outside the boxes by "min" and "max," respectively. POD = probability of detection; FAR = false alarm ratio; ETS = equitable threat score; FOD = flash origin density; E-WRF = explicit lightning forecasting scheme within the Weather Research and Forecasting model.

For grid cells with at least one flash, the POD, FAR, and ETS scores (Lynn et al., 2015) over both land and sea were computed for the simulated FOD fields (Figure 8). As noted above, owing to the low detection efficiency of ZEUS, the lightning forecast evaluation of the lightning places emphasis on grid cells with at least one flash or no flash at all. In other words, the usage of a binary approach (yes or no) emphasizes any lightning occurrences rather than the actual flash rates. The 2-km neighborhood radius was selected because of the overall small displacement errors in the model (Figures 3 and 5). A 6-km radial distance was also evaluated, because it equates the radius of the discharge cylinders. Overall, we notice a slightly lower

performance of the model in predicting lightning activity over the sea. Cases during the warm period exhibit higher POD, lower FAR, and, consequently, higher ETS scores than cold-period cases.

Overall, POD scores are lower than PR92 in Giannaros et al. (2015), but FAR scores are significantly lower for both the warm- and the cold-period cases. For instance, the best POD scores were calculated for the case on 21 September 2011 in both studies, with POD 0.84 and FAR 0.29, compared to 0.95 and 0.72 in Giannaros et al. (2015) respectively.

The statistical diagnostic scheme developed by MC has been widely used, and therefore, is computed here for comparison with the FOD forecasts. To produce lightning, MC assumes a linear combination between the upward graupel mass flux at -15°C and the vertically integrated ice mass within every grid column as a proxy for the bulk effects of electrification. To establish direct comparisons with the forecast statistics for E-WRF, the same verification procedure (i.e., in section 3.2) was utilized for MC. Note that MC flash rates have not been calibrated with the NSSL microphysics scheme, but this should have limited impact on the binary output of flash occurrence.

Compared to E-WRF, MC produces overall larger POD values but also much higher FAR as this algorithm appears to overpredict mean flash densities (Fierro et al., 2013; Lynn et al., 2012; MC). In fact, the absolute number of grid points with simulated flashes with MC is systematically larger than both E-WRF and, thus, the observations (not shown). For one case (29 October 2012) the number of grid points with lightning using the MC algorithm was twice as large compared to E-WRF (i.e., 126,659 versus 66,934). ETS scores in d03 are shown in Figures 9e and 9f, where one can notice the much lower scores for MC, both over land and sea (Figures 8e and 8f). It is relevant to note that MC is designed to be representative of maximum hourly values, which would likely exacerbate any existing systematic overestimation.

The ETS for E-WRF and MC were also computed for 6-hr intervals and for six predefined neighborhood radii ranging between 2 and 12 km by increments of 2 km (Figure 10). The FOD fields for E-WRF produce better scores against MC for all 6-hourly forecast periods and for all radii. A notable peak of ETS is noted for E-WRF during the 1200–1800 accumulation period in the warm-period cases (Figure 10a), when diurnal heating leads to the development of thunderstorms over continental Greece. For MC, maximum ETS values for the warm period are obtained during the 0600–1200 period (Figure 10b), and during 1200–1800 for the cold period (Figure 10d). Both MC and E-WRF show similar timing of the lightning activity during the cold period but different peak times during the warm period.

The calculations of statistical significance of the differences between the qualitative statistical measures for FOD and MC (POD, FAR, and ETS) were conducted by following the approach presented by Hamill (1999). The verification scores were computed for one lightning count threshold after constructing the contingency tables for the 10 case studies. A random sampling of the contingency tables was carried out 10,000 times, using the bootstrapping method proposed by Diaconis and Efron (1983). The statistical significance was performed assuming a 95% confidence interval (variance of 5%), and results showed that all differences between E-WRF and MC were statistically significant (Figure 11).

The lightning forecasts from both E-WRF and MC were verified against ZEUS observations by using a binary approach for simulated and observed lightning strikes. E-WRF tends to outperform MC both in warm-period and cold-period cases, over land and sea. The fractions skill score (FSS; Roberts & Lean, 2008) was computed to provide a more general estimation of the forecast performance for each scheme. This forecast metric is considered more suitable than ETS for displacement errors in the model (Fierro, Clark, et al., 2015; Fierro, Mansell, et al., 2015; Wang et al., 2017; Wilkinson, 2017). The FSS was calculated for the same binary threshold (yes/no) as the other qualitative metrics. The ZEUS observations were used as references, and FSS was calculated for different neighborhood squares, for horizontal scales ranging between 2 and 240 km (i.e., 2, 4, 8, 12, 24, 48, 80,100, 120, and 240 km) for 24-hr forecasts over land and sea aggregated over all cases (Figure 12).

Neighborhood sizes of 50 km (25 grid points) for E-WRF and 180 km (90 grid points) for MC are required to achieve a skillful ($\text{FSS} > 0.5$) lightning/no-lightning discrimination. E-WRF exhibits a notably sharper increase in FSS between the horizontal lengths of 2 and 24 km from about 0.28 to 0.45 compared to an increase from 0.14 to 0.24 for MC. This further supports an overall superior skill for E-WRF in forecasting lightning occurrences. MC shows lower FSS values for the remainder of the neighborhood lengths selected (Figure 12). Using the same verification procedure as for the ETS scores (i.e., bootstrapping), the differences in ETS were found to be statistically significant at 5% variance level.

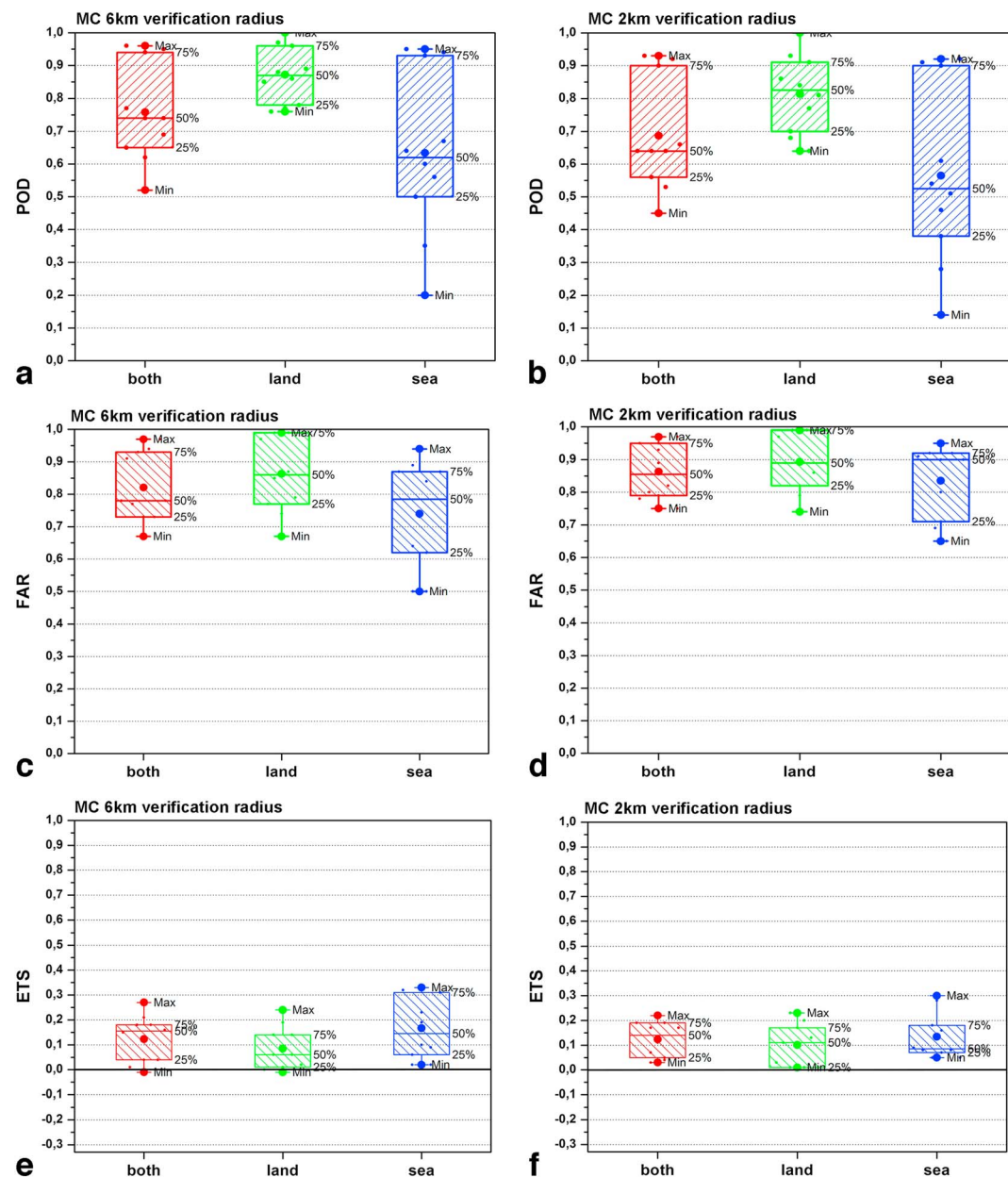


Figure 9. Box and whisker plots of (a, b) POD, (c, d) FAR and (e, f) ETS for the 24-hr accumulated FOD from MC for (a, c, e) 6 km and (b, d, f) 2 km neighborhood radii, for the 10 case studies. Each small colored dot represents the statistical scores of each case study, and the large dot inside the box represents the mean score. The 50% line within the box depicts the median correlation. The boxes are delimited by the lower and upper quartiles (25th and 75th). The 2.5th and 97.5th percentile values are shown at the end bars of the dotted lines outside the boxes by "min" and "max," respectively. POD = probability of detection; FAR = false alarm ratio; ETS = equitable threat score; FOD = flash origin density; MC = McCaul et al. (2009).

As before, the box and whiskers plots of the aggregated FSS for all 10 case studies are shown in 6-hourly intervals in Figure 13 for the neighborhood lengths of 24 km. Warm-period cases exhibit generally higher FSS values for both E-WRF (Figure 13a) and MC (Figure 13b), with the maximum FSS values achieved for 2 July 2010 (0.68 for E-WRF and 0.39 for MC, for the 1200–1800 forecast period). Two of the cold-period cases (18 October 2010 and 6 November 2013, Figures 6a, 6b, 6i, and 6j) produced the lowest FSS values, in agreement with the qualitative metrics of accumulated precipitation forecasts described in section 3.1. These poor forecasts indicate that WRF failed to correctly simulate the spatial and temporal evolution of convection, which negatively impacted the resulting lightning activity.

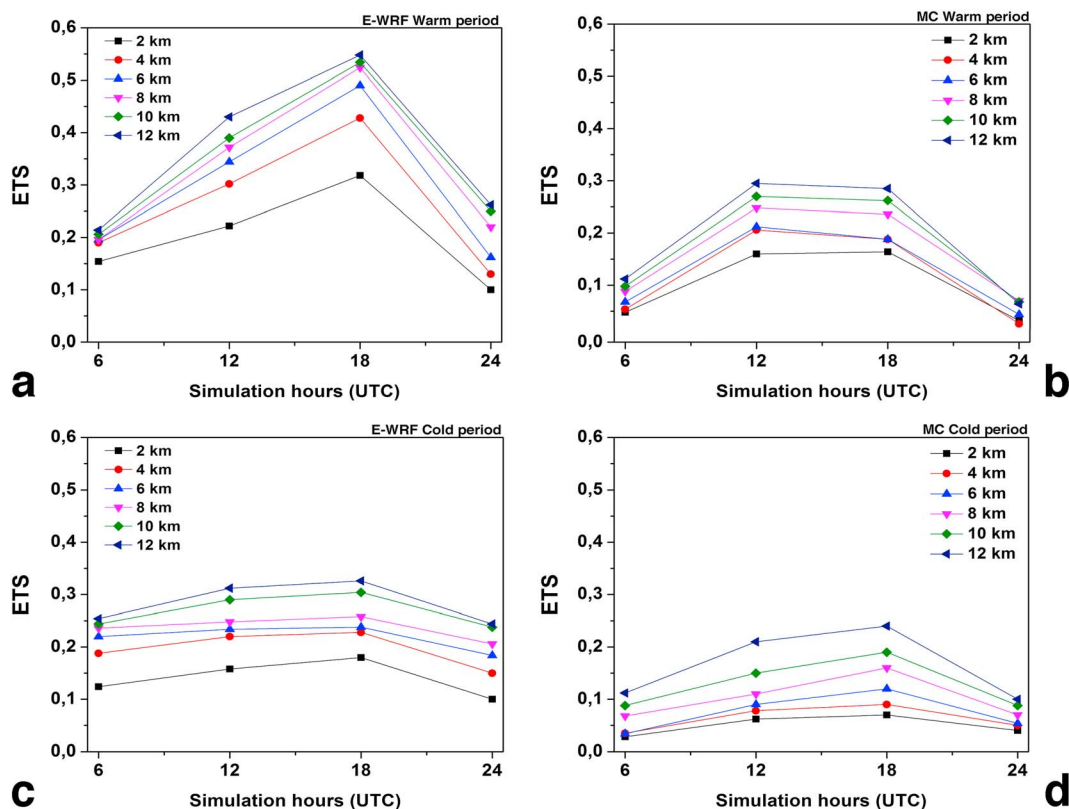


Figure 10. ETS for 6-hourly FOD bins calculated by E-WRF (a, c) and MC (b, d) over the 24-hr forecast period for all six neighborhood radii, averaged for (a, b) the warm-period case studies and (c, d) the cold-period case studies. ETS = equitable threat score; FOD = flash origin density; E-WRF = explicit lightning forecasting scheme within the Weather Research and Forecasting model; MC = McCaul et al. (2009).

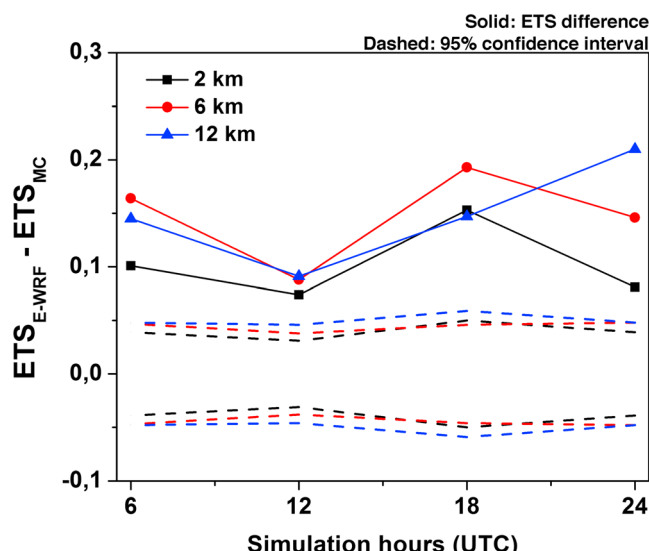


Figure 11. ETS difference for the 6-hr WRF-simulated FOD between E-WRF and MC for the neighborhood radii of 2, 6, and 12 km, overlaid with the 95% confidence interval (dashed line). ETS = equitable threat score; E-WRF = explicit lightning forecasting scheme within the Weather Research and Forecasting model; FOD = flash origin density; MC = McCaul et al. (2009).

4. The Winter Storm “Ariadne”

To provide additional insight of the forecast skill of E-WRF, a strong winter storm with no detected lightning was chosen to evaluate the performance of MC and E-WRF further.

During the beginning of 2017, extremely low temperatures were recorded throughout Greece, as a cold air mass originating from northeastern Europe reached as far south as the Mediterranean Sea. On 9 January 2017, a winter storm named “Ariadne” by NOA caused strong disturbances all over Greece with unusually large accumulations of snow along with freezing conditions. Even areas as far south as Athens were covered with a thick layer of snow overnight (i.e., about 1 m of fresh snow in Skopelos and Kymi). The WRF forecast captured reasonably well the position of the upper-level cutoff low and the occluded front in the Aegean Sea responsible for this unusual snow event over Greece. The model simulated strong convergence zones and steep low-level lapse rates with Convective Available Potential Energy (CAPE) values on the order of 200 J/kg over the Aegean Sea, but no lightning was detected in the actual event.

Figure 14a shows the maximum 24-hr simulated composite reflectivity (dBz) on 9 January 2017. The positively tilted occlusion

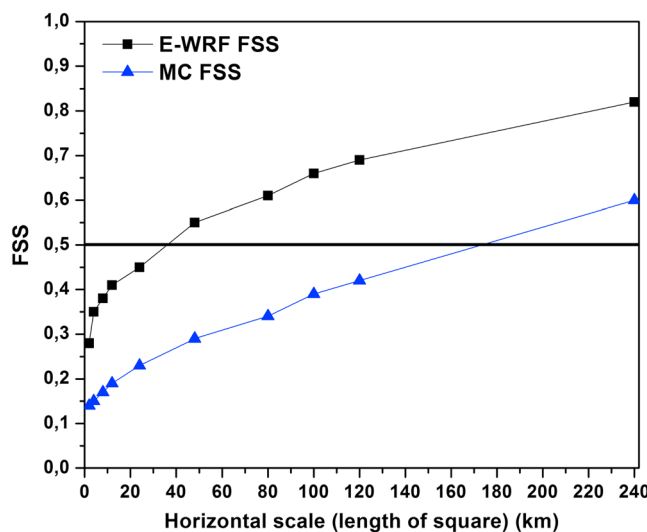


Figure 12. FSS for the 24-hr accumulated lightning forecasts for E-WRF (black line) and MC (blue line) for different neighborhood grid squares aggregated over the 10 case studies herein. FSS = fractions skill score; E-WRF = explicit lightning forecasting scheme within the Weather Research and Forecasting model; MC = McCaul et al. (2009).

attributed to several environmental factors, such as the weakly sheared environment over the sea which reduces the mixed-phased precipitation, or an increasing warm rain process confining the majority of charges to a shallow layer above the freezing level (Fierro & Mansell, 2017). Consequently, the model performance in predicting lightning is superior during the summer when deep convection develops mostly over continental Greece due to thermal instability than in winter when frontal activity results in more thunderstorms over the sea.

A verification procedure was first conducted to evaluate the simulated lightning fields from E-WRF against the ground-based ZEUS lightning detection system. Additionally, the lightning threat diagnostic method of MC was verified against ZEUS observations and the simulated FOD fields from E-WRF. The MC method produced notably more lightning activity than E-WRF because MC assumes the occurrence of lightning

created long-lasting convergence zones over the Aegean Sea where zonally oriented snow bands were developing and growing upscale throughout the day and night hours. ZEUS did not detect any lightning strikes over the aforementioned areas (Figure 14b), suggesting that low-topped convection was not able to build enough charge (and, thus, electric fields) to produce lightning. While E-WRF correctly simulated reasonably the absence of lightning activity (Figure 14d), the MC scheme (Figure 14c) diagnosed widespread FOD up to 15 flashes 24 hr⁻¹. Consistent with the results of Fierro et al. (2013), this experiment illustrates that E-WRF appears to outperform the MC scheme for non-lightning-producing winter events. To assess the robustness of this result, however, a larger sample of similar winter cases, especially with detected lightning, needs to be analyzed in the future.

5. Conclusions and Discussion

The present study evaluated the performance of E-WRF in explicitly forecasting the occurrence of lightning activity, both temporally and spatially for 10 selected high-impact weather cases over Greece. Results for these cases show improved statistical scores for E-WRF (Fierro et al., 2013) compared to the diagnostic schemes (i.e., PR92 and MC). The present analysis also revealed that the modeled lightning activity is more accurately forecast over land than over the sea. This could be

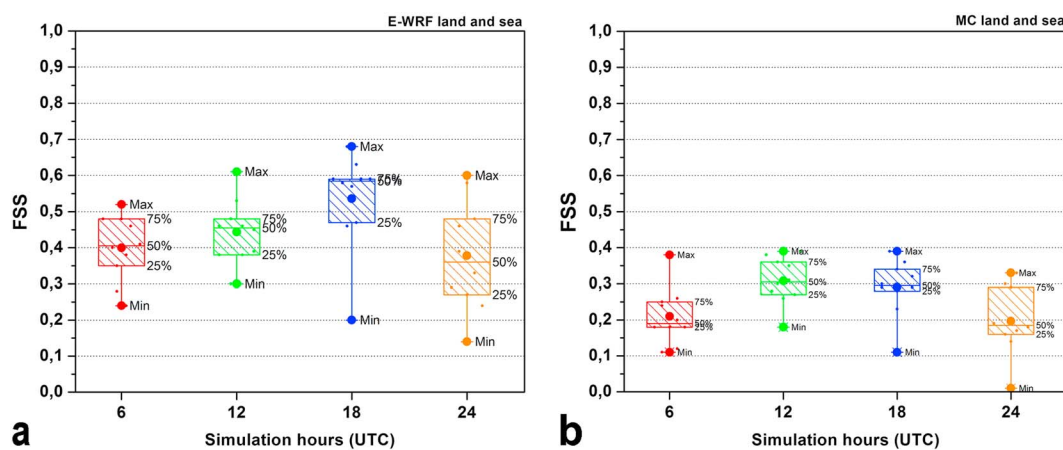


Figure 13. Box and whisker plots of the aggregated FSS for the 6-hr simulated FOD for (a) E-WRF and (b) MC for the 24 km neighborhood length. Each small colored dot represents the statistical scores of each case study, and the large dot inside the box represents the mean score. The 50% line within the box depicts the median correlation. The boxes are delimited by the lower and upper quartiles (25th and 75th). The 2.5th and 97.5th percentile values are shown at the end bars of the dotted lines outside the boxes by "min" and "max," respectively. FSS = fractions skill score; FOD = flash origin density; E-WRF = explicit lightning forecasting scheme within the Weather Research and Forecasting model; MC = McCaul et al. (2009).

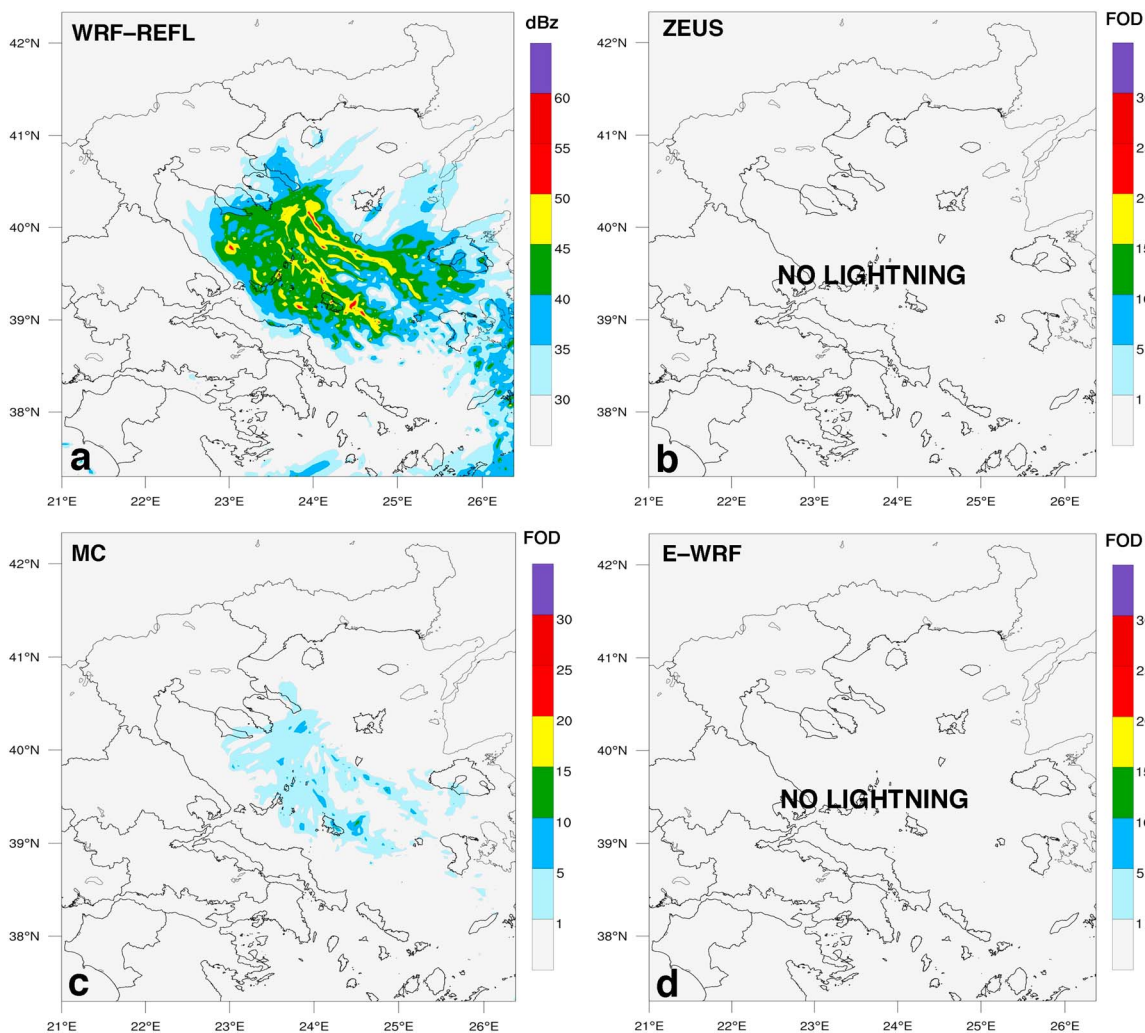


Figure 14. For the case of 9 January 2017 (Ariadne): (a) maximum daily simulated composite reflectivity (dBz) and daily flash origin densities detected by (b) ZEUS and simulated by (c) MC and (d) E-WRF. MC = McCaul et al. (2009); E-WRF = explicit lightning forecasting scheme within the Weather Research and Forecasting model.

whenever given fixed thresholds of graupel and ice fluxes are reached, without taking into account any other details of electrification physics. In addition, lightning in the MC algorithm is calculated by considering the graupel flux within one single layer of the atmosphere, in contrast to E-WRF, which explicitly calculates the electrification rates based on hydrometeor distributions and environmental conditions within each grid cell.

Additional case studies over different geographical areas should be analyzed to further establish the robustness of the results herein and also could examine the role of cloud condensation nucleus concentration in the simulated lightning rates (i.e., Mansell & Ziegler, 2013). The charging physics could also be coupled with other microphysical schemes available as an option in WRF, because the representation of convection (and, thus, lightning) in cloud-resolving simulations may strongly depend on it (Morrison et al., 2012, 2015). Moreover, ground-based systems able to detect total lightning (i.e., GLM and Earth Networks Total Lightning Network (ENTLN)) would be more desirable to more accurately evaluate E-WRF's ability to simulate total lightning activity in terms of spatial and temporal occurrence.

Given these encouraging preliminary set of results coupled with the low computational cost of E-WRF, plans are underway to install and run E-WRF operationally at the NOA, replacing the current operational setup which utilizes the modified PR92 parameterization based on Giannaros et al. (2015) configuration.

Acknowledgments

This research has been partly financed by the "Development Proposals of Research Entities—KRIPIIS II" framework, which is funded by N.P.

"Competitiveness and Entrepreneurship 2014–2020", Action: "THESPIAN II – Development of synergistic and integrated methods and tools for monitoring, management and forecasting of Environmental parameters and pressures". Funding was also provided by NOAA/Office of Oceanic and Atmospheric Research under NOAA-University of Oklahoma Cooperative Agreement

NA11OAR4320072, U.S. Department of Commerce. This work was further supported by the U.S. Department of Commerce (NOAA) under the GOES-R Risk Reduction Program. The simulations were made possible through computing resources provided by the National Observatory of Athens (NOA). Lightning data from ZEUS are available from the website of NOA (http://www.thunderstorm24.com/historical_maps_eu-en.cfm) or upon request. Precipitation data are also available online from NOA (<http://stratus.meteo.noa.gr/front>).

References

- Casati, B., Wilson, L. J., Stephenson, D. B., Nurmi, P., Ghelli, A., Pocernich, M., et al. (2008). Forecast verification: Current status and future directions. *Meteorological Applications*, 15, 3–18. <https://doi.org/10.1002/met.52>
- Chen, F., & Dudhia, J. (2001). Coupling an advanced land surface-hydrology model with the Penn State-NCAR MM5 modeling system. Part I: Model implementation and sensitivity. *Monthly Weather Review*, 129, 569–585.
- Clark, A. J., & Weisman, M. L. (2010). Neighborhood-based verification of precipitation forecasts from convection-allowing NCAR WRF model simulations and the operational NAM. *Weather and Forecasting*, 25, 1495–1509. <https://doi.org/10.1175/2010WAF2222404.1>
- Dendy, J. E. Jr. (1987). Two multigrid methods for three-dimensional problems with discontinuous and anisotropic coefficients. *SIAM Journal on Scientific and Statistical Computing*, 8, 673–685.
- Dendy, J. E. Jr., & Moulton, J. D. (2010). Black box multigrid with coarsening by a factor of three. *Numerical Linear Algebra with Applications*, 17, 577–598.
- Diaconis, P., & Efron, B. (1983). Computer-intensive methods in statistics. *Scientific American*, 248(5), 116–130.
- Dotzek, N., Groenemeijer, P., Feuerstein, B., & Holzer, A. M. (2009). Overview of ESSL's severe convective storms research using the European severe weather database ESWD. *Atmospheric Research*, 93, 575–586.
- Drobinski, P., Ducrocq, V., Alpert, P., Anagnostou, E., Béranger, K., et al. (2014). HyMeX: A 10-year multidisciplinary program on the Mediterranean water cycle. *Bulletin of the American Meteorological Society*, 95, 1063–1082.
- Dudhia, J. (1989). Numerical study of convection observed during the winter monsoon experiment using a mesoscale two-dimensional model. *Journal of the Atmospheric Sciences*, 46, 3077–3107.
- Dwyer, J. R. (2003). A fundamental limit on electric fields in air. *Geophysical Research Letters*, 30, 2055. <https://doi.org/10.1029/2003GL017781>
- Ebert, E. E. (2009). Neighborhood verification: A strategy for rewarding close forecasts. *Weather and Forecasting*, 24, 1498–1510. <https://doi.org/10.1175/2009WAF222251.1>
- Federico, S., Avolio, E., Bellecci, C., Colacino, M., Lavagnini, A., Accadria, C., et al. (2004). Three model intercomparison for quantitative precipitation forecast over Calabria. *Il Nuovo Cimento C*, 27, 627–647.
- Fierro, A. O., Clark, A. J., Mansell, E. R., MacGorman, D. R., Dembek, S., & Ziegler, C. (2015). Impact of storm-scale lightning data assimilation on WRF-ARW precipitation forecasts during the 2013 warm season over the contiguous United States. *Monthly Weather Review*, 143, 757–777.
- Fierro, A. O., Gilmore, M. S., Mansell, E. R., Wicker, L. J., & Straka, J. M. (2006). Electrification and lightning in an idealized boundary-crossing supercell simulation of 2 June 1995. *Monthly Weather Review*, 134(11), 3149–3172.
- Fierro, A. O., & Mansell, E. R. (2017). Electrification and lightning idealized simulations of a hurricane-like vortex subject to wind shear and sea surface temperature cooling. *Journal of the Atmospheric Sciences*, 74(6), 2023–2041.
- Fierro, A. O., Mansell, E. R., MacGorman, D. R., & Ziegler, C. (2015). Explicitly simulated electrification and lightning within a tropical cyclone based on the environment of Hurricane Isaac (2012). *Journal of the Atmospheric Sciences*, 72, 4167–4193.
- Fierro, A. O., Mansell, E. R., MacGorman, D. R., & Ziegler, C. L. (2013). The implementation of an explicit charging and discharge lightning scheme within the WRF-ARW model: Benchmark simulations of a continental squall line, a tropical cyclone, and a winter storm. *Monthly Weather Review*, 141, 2390–2415.
- Giannaros, T. M., Kotroni, V., & Lagouvardos, K. (2015). Predicting lightning activity in Greece with the Weather Research and Forecasting (WRF) model. *Atmospheric Research*, 156, 1–13.
- Giannaros, T. M., Lagouvardos, K., & Kotroni, V. (2016). Performance evaluation of an operational lightning forecasting system in Europe. *Natural Hazards*, 1–18. <https://doi.org/10.1007/s11069-016-2555-y>
- Gish, O. H. (1944). Evaluation and interpretation of the columnar resistance of the atmosphere. *Journal of Geophysical Research*, 49, 159–168.
- Goodman, S. J., Blakeslee, R. J., Koshak, W. J., Mach, D., Bailey, J., Buechler, D., et al. (2013). The GOES-R Geostationary Lightning Mapper (GLM). *Atmospheric Research*, 125–126, 34–49. <https://doi.org/10.1016/j.atmosres.2013.01.006>
- Goodman, S. J., DeMaria, M., Schmidt, T. J., Mostek, A., Jedlovec, G., Siewert, C., et al. (2012). The GOES-R proving ground: Accelerating user readiness for the next-generation geostationary environmental satellite system. *Bulletin of the American Meteorological Society*, 93, 1029–1040. <https://doi.org/10.1175/BAMS-D-11-00175.1>
- Grell, G. A., & Devenyi, D. (2002). A generalized approach to parameterizing convection combining ensemble and data assimilation techniques. *Geophysical Research Letters*, 29, L15311. <https://doi.org/10.1029/2002GL015311>
- Hamill, T. M. (1999). Hypothesis tests for evaluating numerical precipitation forecasts. *Weather and Forecasting*, 14, 155–167.
- Hong, S. Y., Noh, Y., & Dudhia, J. (2006). A new vertical diffusion package with an explicit treatment of entrainment processes. *Monthly Weather Review*, 134, 2318–2341.
- Karagiannidis, A., Lagouvardos, K., Kotroni, V., & Mazarakis, N. (2016). Investigation of single-cell thunderstorms lightning activity using METEOSAT rapid scan infrared imagery. *International Journal of Remote Sensing*, 37(20), 5001–5020.
- Kotroni, V., & Lagouvardos, K. (2008). Lightning occurrence in relation with elevation, terrain slope and vegetation cover in the Mediterranean. *Journal of Geophysical Research*, 113, D21118. <https://doi.org/10.1029/2008JD010605>
- Lagouvardos, K., Kotroni, V., Betz, H. D., & Schmidt, K. (2009). A comparison of lightning data provided by ZEUS and LINET networks over Western Europe. *Natural Hazards and Earth System Sciences*, 9, 1713–1717.
- Lagouvardos, K., Kotroni, V., Bezes, A., Koletsis, I., Kopania, T., et al. (2017). The automatic weather stations NOANN network of the National Observatory of Athens: Operation and database. *Geoscience Data Journal*, 4(1), 4–16.
- Lagouvardos, K., Kotroni, V., Koussis, A., Feidas, C., Buzzi, A., & Malguzzi, P. (2003). The meteorological model BOLAM at the National Observatory of Athens: Assessment of two-year operational use. *Journal of Applied Meteorology*, 42, 1667–1678.
- Lynn, B. H., Kelman, G., & Ellrod, G. (2015). An evaluation of the efficacy of using observed lightning to improve convective lightning forecasts. *Weather and Forecasting*. <https://doi.org/10.1175/WAF-D-13-00028.1>
- Lynn, B. H., Yair, Y., Price, C., Kelman, G., & Clark, A. J. (2012). Predicting cloud-to-ground and intracloud lightning in weather forecast models. *Weather and Forecasting*, 27, 1470–1488. <https://doi.org/10.1175/WAF-D-11-00144.1>
- MacGorman, D. R., & Rust, W. D. (1998). *The electrical nature of storms* (p. 422). New York: Oxford University Press.
- Mansell, E. R., MacGorman, D. R., Ziegler, C. L., & Straka, J. M. (2005). Charge structure and lightning sensitivity in a simulated multicell thunderstorm. *Journal of Geophysical Research*, 110, D12101. <https://doi.org/10.1029/2004JD005287>
- Mansell, E. R., & Ziegler, C. L. (2013). Aerosol effects on simulated storm electrification and precipitation in a two-moment bulk microphysics model. *Journal of the Atmospheric Sciences*, 70, 2032–2050. <https://doi.org/10.1175/JAS-D-12-0264.1>
- Mansell, E. R., Ziegler, C. L., & Bruning, E. C. (2010). Simulated electrification of a small thunderstorm with two-moment bulk microphysics. *Journal of the Atmospheric Sciences*, 67, 171–194.

- Mazarakis, N., Kotroni, V., Lagouvardos, K., & Argiriou, A. (2008). Storms and lightning activity in Greece during the warm period of 2003–06. *Journal of Applied Meteorology*, 47, 3089–3098.
- Mazarakis, N., Kotroni, V., Lagouvardos, K., & Argiriou, A. A. (2009). The sensitivity of numerical forecasts to convective parameterization during the warm period and the use of lightning data as an indicator for convective occurrence. *Atmospheric Research*, 94, 704–714.
- McCaull, E. W., Goodman, S. J., LaCasse, K. M., & Cecil, D. J. (2009). Forecasting lightning threat using cloud-resolving model simulations. *Weather and Forecasting*, 24, 709–729.
- Metzger, E., & Nuss, W. A. (2013). The relationship between total cloud lightning behavior and radar-derived thunderstorm structure. *Weather and Forecasting*, 28, 237–253. <https://doi.org/10.1175/WAF-D-11-00157.1>
- Mlawer, E. J., Taubman, S. J., Brown, P. D., Iacono, M. J., & Clough, S. A. (1997). Radiative transfer for inhomogeneous atmosphere: RRTM, a validated correlated-k model for the longwave. *Journal of Geophysical Research*, 102, 16,663–16,682.
- Morgan, D., Hardwick, C., Haigh, S., & Meakins, A. (2012). *The interaction of lightning with aircraft and the challenges of lightning testing, lightning hazards to aircraft and launchers* (pp. 05–11). AL: Journal Aerospace Lab.
- Morrison, H., Morales, A., & Villanueva-Birriel, C. (2015). Concurrent sensitivities of an idealized deep convective storm to parameterization of microphysics, horizontal grid resolution, and environmental static stability. *Monthly Weather Review*, 143, 2082–2104. <https://doi.org/10.1175/MWR-D-14-00271.1>
- Morrison, H., Tessendorf, S. A., Ikeda, K., & Thompson, G. (2012). Sensitivity of a simulated midlatitude squall line to parameterization of raindrop breakup. *Monthly Weather Review*, 140, 2437–2460.
- Pinty, J.-P., & Barthe, C. (2008). Ensemble simulation of the lightning flash variability in a 3D cloud model with parameterizations of cloud electrification and lightning flashes. *Monthly Weather Review*, 136, 380–387.
- Price, C., & Rind, D. (1992). A simple lightning parameterization for calculating global lightning distributions. *Journal of Geophysical Research*, 97, 9919–9933.
- Pytharoulis, I., Kotsopoulos, S., Tegoulias, I., Kartsios, S., Bampzelis, D., & Karacostas, T. (2016). Numerical modeling of an intense precipitation event and its associated lightning activity over northern Greece. *Atmospheric Research*, 169, 523–538. <https://doi.org/10.1016/j.atmosres.2015.06.019>
- Ribaudo, J. F., Bousquet, O., Coquillat, S., Al-Sakka, H., Lambert, D., Ducrocq, V., & Fontaine, E. (2015). Evaluation and application of hydro-meteor classification algorithm outputs inferred from multi-frequency dual polarimetric radar observations collected during HyMeX. *Quarterly Journal of the Royal Meteorological Society*, 142, 95–107.
- Rison, W., Thomas, R. J., Krebsiel, P. R., Hamlin, T., & Harlin, J. (1999). A GPS-based three-dimensional lightning mapping system: Initial observations in central New Mexico. *Geophysical Research Letters*, 26, 3573–3576.
- Roberts, N. M., & Lean, H. W. (2008). Scale-selective verification of rainfall accumulations from high-resolution forecasts of convective events. *Monthly Weather Review*, 136, 78–97. <https://doi.org/10.1175/2007MWR2123.1>
- Rudlosky, S., Peterson, M. J., & Kahn, D. T. (2017). GLD360 performance relative to TRMM LIS. *Journal of Atmospheric and Oceanic Technology*, 34, 1307–1322. <https://doi.org/10.1175/JTECH-D-16-0243.1>
- Rudlosky, S., & Shea, D. T. (2013). Evaluating WWLLN performance relative to TRMM/LIS. *Geophysical Research Letters*, 40, 2344–2348. <https://doi.org/10.1002/grl.50428>
- Saunders, C. P. R., & Peck, S. L. (1998). Laboratory studies of the influence of the rime accretion rate on charge transfer during crystal/graupe collisions. *Journal of Geophysical Research*, 103, 13,949–13,956.
- Schultz, C. J., Petersen, W. A., & Carey, L. D. (2011). Lightning and severe weather: A comparison between total and cloud-to-ground lightning trends. *Weather and Forecasting*, 26, 744–755.
- Schwartz, C. S., Kain, J. S., Weiss, S. J., Xue, M., Bright, D. R., Kong, F., et al. (2010). Toward improved convection-allowing ensembles: Model physics sensitivities and optimizing probabilistic guidance with small ensemble membership. *Weather and Forecasting*, 25, 263–280. <https://doi.org/10.1175/2009WAF2222267.1>
- Skamarock, W. C., & Klemp, J. B. (2008). A time-split nonhydrostatic atmospheric model for weather research and forecasting applications. *Journal of Computational Physics*, 227, 3465–3485. <https://doi.org/10.1016/j.jcp.2007.01.037>
- Takahashi, T. (1978). Riming electrification as a charge generation mechanism in thunderstorms. *Journal of the Atmospheric Sciences*, 35, 1536–1548. <https://doi.org/10.1175/1520>
- Wang, H., Liu, Y., Cheng, W. Y. Y., Zhao, T., Xu, M., Liu, Y., et al. (2017). Improving lightning and precipitation prediction of severe convection using lightning data assimilation with NCAR WRF-RTFDDA. *Journal of Geophysical Research: Atmospheres*, 122, 12,296–12,316. <https://doi.org/10.1002/2017JD027340>
- Wiens, K. C., Rutledge, S. A., & Tessendorf, S. A. (2005). The 29 June 2000 supercell observed during STEPS. Part II: Lightning and charge structure. *Journal of the Atmospheric Sciences*, 62, 4151–4177. <https://doi.org/10.1175/JAS3615.1>
- Wilkinson, J. M. (2017). A technique for verification of convection-permitting NWP model deterministic forecasts of lightning activity. *Weather and Forecasting*, 32, 97–115. <https://doi.org/10.1175/WAF-D-16-0106.1>
- Williams, E., Boldi, B., Matlin, A., Weber, M., Hodanish, S., Sharp, D., et al. (1999). The behavior of total lightning activity in severe Florida thunderstorms. *Atmospheric Research*, 51(3), 245–265.
- Wong, J., Barth, M. C., & Noone, D. (2013). Evaluating a lightning parameterization based on cloud-top height for mesoscale numerical model simulations. *Geoscientific Model Development*, 6, 429–443.
- Yair, Y., Lynn, B., Price, C., Kotroni, V., Lagouvardos, K., Morin, E., et al. (2010). Predicting the potential for lightning activity in Mediterranean storms based on the Weather Research and Forecasting (WRF) model dynamic and microphysical fields. *Journal of Geophysical Research*, 115, D04205. <https://doi.org/10.1029/2008JD010868>
- Yang, J., Zhang, Z., Wei, C., Lu, F., & Guo, Q. (2017). Introducing the new generation of Chinese geostationary weather satellites, Fengyun-4. *Bulletin of the American Meteorological Society*, 98, 1637–1659. <https://doi.org/10.1175/BAMS-D-16-0065.1>
- Zhang, D. L., & Anthes, R. A. (1982). A high-resolution model of the planetary boundary layer—Sensitivity tests and comparisons with SESAME-79 data. *Journal of Applied Meteorology*, 21, 1594–1609.
- Ziegler, C. L., & MacGorman, D. R. (1994). Observed lightning morphology relative to modeled space charge and electric field distributions in a tornadic storm. *Journal of the Atmospheric Sciences*, 51, 833–851.
- Ziegler, C. L., MacGorman, D. R., Dye, J. E., & Ray, P. S. (1991). A model evaluation of non-inductive graupel-ice charging in the early electrification of a mountain thunderstorm. *Journal of Geophysical Research*, 96, 12,833–12,855.